Check for updates

Advanced Materials

ADVANCED MATERIALS
www.advmat.de

RESEARCH ARTICLE

Durable Interphase Engineering on SiO_x Anodes Through Interfacial-Enrichment-Facilitated Polymerization

Shiming Chen[1] | Kai Yang[2] | Wenguang Zhao[1] | Wei Yang[3] | Jiangxiao Li[4] | Chenyu Yang[4] | Zhikang Deng[1] | Yue Zuo[1] | Xiaohu Wang[1] | Zu-Wei Yin[5] | Junyang Liu[6] | Meng Zhang[7] | Feng Pan[1] | Luyi Yang[1]

[1]School of Advanced Materials, Peking University Shenzhen Graduate School, Shenzhen, People's Republic of China | [2]Department of Electrical and Electronic Engineering, Advanced Technology Institute, University of Surrey, Guildford, Surrey, UK | [3]Materials Innovation Institute for Life Sciences and Energy (MILES), The University of Hong Kong-SIRI, Shenzhen, China | [4]National Synchrotron Radiation Laboratory, University of Science and Technology of China, Hefei, People's Republic of China | [5]College of Energy, Xiamen University, Xiamen, People's Republic of China | [6]College of Chemistry and Chemical Engineering, Xiamen University, Xiamen, People's Republic of China | [7]BTR New Material Group Co., Ltd., Shenzhen, China

Correspondence: Luyi Yang (yangly@pkusz.edu.cn)

Received: 7 March 2026 | **Revised:** 7 July 2026 | **Accepted:** 28 July 2026

Keywords: cycle stability | inner Helmholtz plane | interfacial reaction | SiO_x anode | solid electrolyte interphase

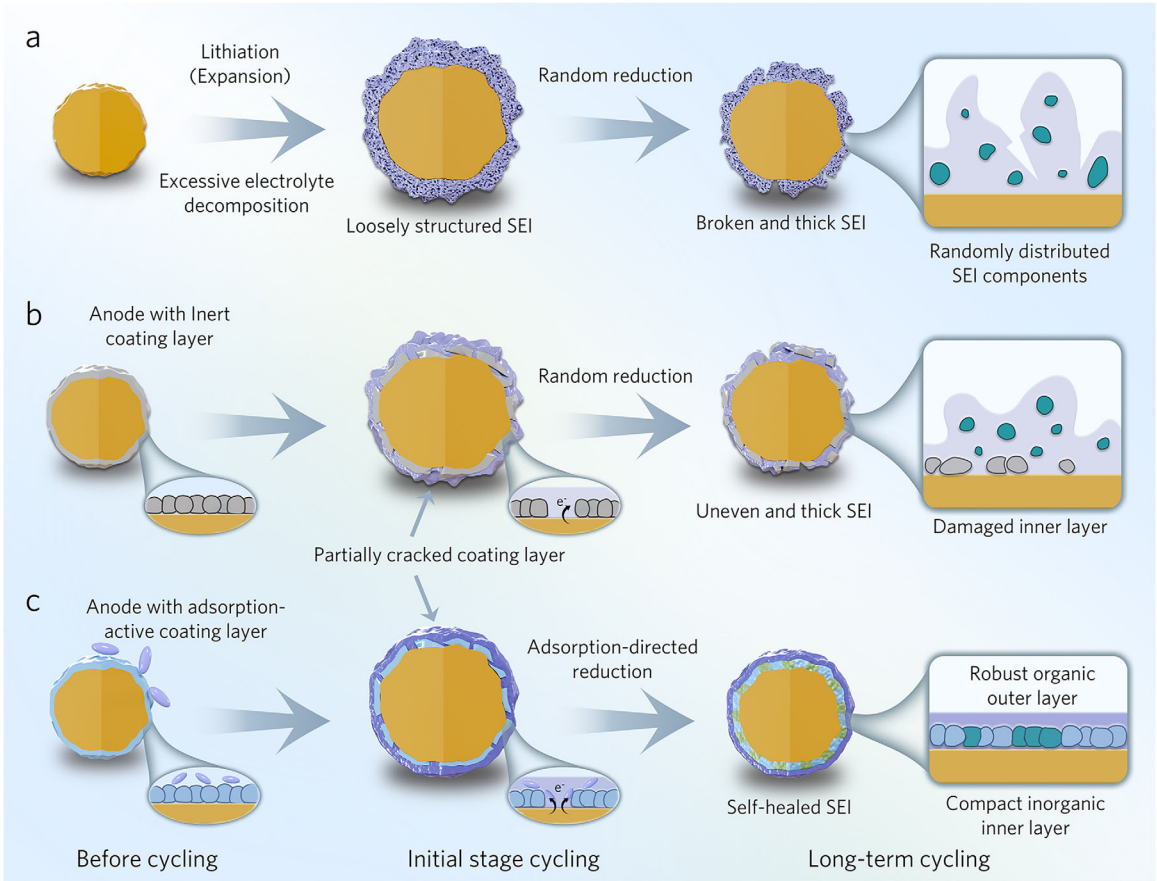
ABSTRACT

Constructing a robust solid electrolyte interphase (SEI) is a proven strategy to enhance the performance of Si-based anodes by accommodating severe volume swings and suppressing interfacial side reactions. However, existing strategies that rely solely on either chemical coating or electrochemical formation struggle to reconcile SEI uniformity and long-term stability. Here, we propose a synergistic strategy that integrates the interfacial modification with in situ regulated electrolyte decomposition. A conformal layer composed of LiF and Li_3PO_4 is pre-formed on SiO_x anodes, where LiF serves as a stable mechanical framework for the inorganic-rich SEI, and Li_3PO_4 selectively adsorbs fluoroethylene carbonate (FEC), favoring the polymerization of FEC-derived species via interfacial enrichment to form the high-molecular-weight organic species. These electrochemically generated SEI components effectively compensate for the damage to the initial coating caused by volume expansion, enabling the SEI to possess both structural integrity and resilience. Consequently, the modified SiO_x anode exhibits benchmark electrochemical performance, delivering excellent cycling stability (1086 mA h g^{-1}, 81% capacity retention for 300 cycles at 0.8 A g^{-1}) and high-rate capability (1010 mAh g^{-1} at 2.4 A g^{-1}). This work establishes a precedent for the dynamic repair interphase design paradigm for high-capacity anodes.

1 | Introduction

With the continuous increasing demand for high-energy-density and low-cost lithium-ion batteries (LIBs), silicon suboxide (SiO_x, $0< x < 2$) has emerged as promising candidate for next-generation anodes due to its high theoretical capacity (~1500 mAh g^{-1}), appropriate operation voltage (~0.2 V vs. Li/Li^+) and abundant resources [1, 2]. However, SiO_x suffers from significant volume variation (~130%) during cycling, resulting in numerous side effects. Specifically, the solid electrolyte interphase (SEI), formed through the electrochemical reduction of conventional carbonate-based electrolytes, often exhibits solvent-swelling loose structures, which cannot accommodate the volume swing of SiO_x anodes [3]. Therefore, the SEI is repeatedly damaged and reconstructed during cycles, causing irreversible thickening and eventually leading to the degradation of battery performance. To address the aforementioned issues, it is essential to construct a stable SEI layer with excellent chemical and mechanical stability on the anode surface [4–8].

All rights reserved, including rights for text and data mining and training of artificial intelligence technologies or similar technologies.
© 2026 Wiley-VCH GmbH



SCHEME 1 | Schematic illustration of SEI design principle for Si-based anodes.

Hitherto, numerous inorganic species (e.g., LiF, Li_3PO_4 and Li_2O) have been identified as effective SEI components to stabilize the interface due to their desirable physicochemical properties compared with organic ones [9–12]. For instance, LiF possesses high Young's modulus (~125 GPa), high interfacial energy (73.28 meV $Å^{-2}$) and low electronic conductivity (band gap = 8.72 eV) which contribute to accommodate deformation of Si-based anodes and passivate interface during cycling effectively [13–15]. Besides, suitable ion conductors such as Li_3PO_4 (~10^{-6} S cm^{-1}) could promote Li^+ desolvation kinetics within the SEI due to its low work function [11]. Previous studies have shown that SEI layers containing the aforementioned inorganic components can be constructed via electrolyte modification [16, 17] or artificial coating [18, 19], effectively suppressing the detrimental effects of volume swings and enhancing the electrochemical performance of anodes [20].

However, the SEI formation through electrochemical decomposition of electrolyte is a heterogeneous reaction governed by various thermodynamic and kinetic factors [21]. As shown in Scheme 1a, from an electrochemical perspective, a truly uniform SEI is fundamentally unattainable, as its formation is governed by localized, non-equilibrium interfacial reactions coupled with heterogeneous electron/ion transport and path-dependent growth kinetics [22]. In contrast, surface coating strategies (Scheme 1b) enable better initial control but are typically damaged upon lithiation and lack self-healing capability. Therefore, relying solely on electrolyte modification or interfacial coating presents inherent limitations. To address these challenges, a promising approach lies in the preemptive and controllable construction of an SEI layer on the anode surface, which can subsequently be refined and reinforced by electrolyte decomposition during cycling (Scheme 1c) [23]. Beyond merely offering passive shielding, the pre-formed SEI should enable spontaneous active remediation upon cycling degradation. The interface chemistry between the electrode and electrolyte also plays an essential role in regulating the SEI formation [24, 25]. Therefore, the pre-formed SEI should ideally exhibit the ability to promote the decomposition of SEI-forming species, thereby accelerating and directing the construction of a stable interphase.

Different from passive reliance on electrolyte decomposition and one-time artificial coatings without repair capability, this work proposes a strategy for dynamic repair and reinforcement of the SEI layer, which enables selective adsorption at the inner Helmholtz plane (IHP) and guides interfacial reaction pathways through the surface LiF–Li_3PO_4 coating. In the pre-coating layer, LiF provides a stable foundation for the subsequent growth of SEI, while Li_3PO_4 selectively adsorbs FEC, enabling its preferential and directed involvement in the electrochemical SEI formation process. Besides, the enrichment of FEC on the electrode surface facilitates polymerization reactions to produce high-molecular-weight organic SEI species. The broken coating layer cycling was repaired by regulated electrochemical decomposition, mainly composed of LiF and polymers. Through this design strategy throughout the whole life cycle, an SEI consisting of a

15214095, 0, Downloaded from https://advanced.onlinelibrary.wiley.com/doi/10.1002/adma.74536 by University Town Of Shenzhen, Wiley Online Library on [08/09/2026]. See the Terms and Conditions (https://onlinelibrary.wiley.com/terms-and-conditions) on Wiley Online Library for rules of use; OA articles are governed by the applicable Creative Commons License

well-distributed LiF and Li_3PO_4 inorganic inner layer and an elastic organic outer layer was obtained, exhibiting superior mechanical stability and Li^+ conductivity. Consequently, the resulting anode demonstrated a high average cyclic Coulombic efficiency (CE) of 99.7% and outstanding rate performance (1010 mAh g^{-1} at 2.4 A g^{-1}). In addition, the proposed strategy enables Ah-level pouch cells containing 30 wt.% SiO_x materials to achieve excellent cycling stability, with 80.1% capacity retention at 0.5C after 1000 cycles. This study proposes an innovative design principle for stable interphases within battery systems. Specifically, target interphases are required to simultaneously afford passive interfacial shielding and trigger spontaneous electrochemical remediation via active induction.

2 | Results and Discussion

2.1 | Surface-Engineering for SiOx Anode

As discussed above, heterogeneous electrochemical reactions, such as SEI formation, are highly uncontrollable due to their susceptibility to factors like electrode surface inhomogeneity and the different reactivity of electrolyte components. These facts make it extremely difficult to form a uniform and dense SEI layer (Figure S1). Artificially constructing a dense and inorganic-rich inner layer through chemical reactions before electrochemical cycling would provide a stable framework for subsequent SEI formation. During the initial lithiation process, the volume expansion of SiO_x would inevitably disrupt the dense coating layer formed through chemical synthesis, while the species derived from electrolyte decomposition fill in the emerging cracks. Ideally, crack-filling species should also be relatively stable inorganic compounds, enabling the formation of a robust SEI that could effectively passivate SiO_x surface and support dynamic repair and reinforcement of the interphase (Figure S2). However, traditional carbonate solvent molecules typically decompose into Li_2CO_3 and lithium ethylene decarbonate (LEDC), which exhibit poor mechanical properties and low ionic conductivity (Figure S3) [26, 27]. In contrast, FEC is a desirable electrolyte additive, as it decomposes into high Young's modulus LiF and elastic polymers [28–31], providing both structural stability and flexibility. Hence, increasing the occupation number of FEC molecules in the IHP is a crucial strategy to enhance its decomposition efficiency.

Firstly, density functional theory (DFT) calculations were carried out to evaluate the binding capability of different surfaces with FEC molecules. Combing with results of x-ray photoelectron spectroscopy (XPS) and high-resolution transmission electron microscopy (HRTEM), the surface of pristine SiO_x is primarily composed of tetravalent silicon (Figure S4) with a layer of graphitized carbon coating (Figure S5). Hence, graphite and SiO_2 were employed to represent the simplified surface structure of SiO_x and its carbon coating layer for calculation, consistent with modeling strategies adopted in previous studies [32]. The calculation results show that Li_3PO_4 surface exhibits highest binding energy (−1.31 eV) with FEC than that of SiO_2, C and LiF, suggesting that Li_3PO_4 could achieve a FEC-enriched IHP (Figure 1a). Furthermore, the detailed adsorption behavior of FEC on various solid surfaces was investigated through molecular dynamics (MD) simulation (Figure S6). The results show that more FEC molecules accumulate on the Li_3PO_4 surface, confirming its superior affinity with FEC. And LiF serves as a mechanically stable framework within the SEI, providing structural integrity and electronic insulation to maintain interfacial stability. In addition, the edge structure of Li_3PO_4 shows a significantly higher Fermi energy level (−1.7 eV) than SiO_2 (−4.4 eV), C (−2.5 eV) and LiF (−5.1 eV), suggesting its superior reactivity for the reductive decomposition of FEC (Figure S7) [33]; correspondingly, the dissociation energy for ring-opening reaction of FEC on the Li_3PO_4 surface is also relatively lower than those on other surfaces (Figure S8). Both results demonstrate that, beyond surface adsorption, Li_3PO_4 can also accelerate the direct ring-opening reduction of FEC on its surface.

Based on the above calculation results, LiF and Li_3PO_4 are identified as the ideal coating layer components for SiO_x material. By uniformly mixing LiOH, $NH_4H_2PO_4$ and NH_4F through a liquid-phase method and subsequently forming the coating layer through solid-phase sintering in an Ar atmosphere, a scalable synthesis route can be achieved. In addition, the waste liquid generated from the reaction is aqueous ammonia, which is relatively easy to dispose of. The surface-optimized SiO_x material (~5 μm, denoted by SiO_x@FP, Figure 1b and Figure S9) contains coating agents at approximately 2% of the total mass, resulting in a negligible effect on the specific capacity. The more detailed synthesis method is provided in the Supporting Information. From the x-ray diffraction (XRD) patterns, sharp diffraction peaks corresponding to LiF and Li_3PO_4 crystalline facets can be observed, suggesting that LiF and Li_3PO_4 crystal were successfully formed on SiO_x (Figure S10). This result is supported by HRTEM images (Figure S11), where lattice diffraction fringes of LiF and Li_3PO_4 can be detected and crystals exhibit island-like distribution in the coating layer. Combining the energy-dispersive x-ray spectroscopy (EDS) mapping with different scales, a homogeneous distribution of F and P elements can be observed on the surface of the SiO_x@FP particle (Figure 1c, Figures S12 and S13). Additionally, XPS and soft x-ray absorption spectroscopy (sXAS) results (Figures S14 and S15) not only confirm the existence of LiF and Li_3PO_4 species on the SiO_x@FP surface but also exhibit the P–F bond and O–P–F bond signals indicates that Li_3PO_4 domains are bonded to LiF, contributing to a robust inorganic layer [34–36]. According to the Brunauer–Emmett–Teller (BET) test results (Figure S16), the coating layer has little effect on the specific surface area, which might potentially influence the structure of IHP. Then crushing tests of single particles for two materials were measured (Figure 1d). It can be clearly observed that the maximum tolerance force of single particle was significantly improved of SiO_x@FP (36.2 mN) compared with pristine SiO_x (26.7 mN), suggesting that this mechanical robust protective layer helps disperse the surface stress of SiO_x particles [4]. To verify the adsorption behavior of FEC on the SiO_x@FP surface, the ex situ Fourier transform infrared spectroscopy (FTIR) of different electrodes wetted by electrolyte before cycling was investigated (Figure 1e). The intensified peaks corresponding to the deformation of the C–F bond (ν C–F, 1110 cm^{-1}) and the stretching vibration of the C–F bond (δ C–F, 1150 cm^{-1}) prove the enhanced FEC adsorption behavior on the SiO_x@FP surface [37]. To further evaluate individual roles of LiF and Li_3PO_4, the same measurements were conducted on control SiO_x anodes coated exclusively with LiF or Li_3PO_4 (denoted as SiO_x@F or SiO_x@P, respectively). Combing the results of XRD, XPS and EDS, SiO_x@F and SiO_x@P anodes were successfully synthesized and applied in

15214095, 0, Downloaded from https://advanced.onlinelibrary.wiley.com/doi/10.1002/adma.74536 by University Town Of Shenzhen, Wiley Online Library on [08/09/2026]. See the Terms and Conditions (https://onlinelibrary.wiley.com/terms-and-conditions) on Wiley Online Library for rules of use; OA articles are governed by the applicable Creative Commons License

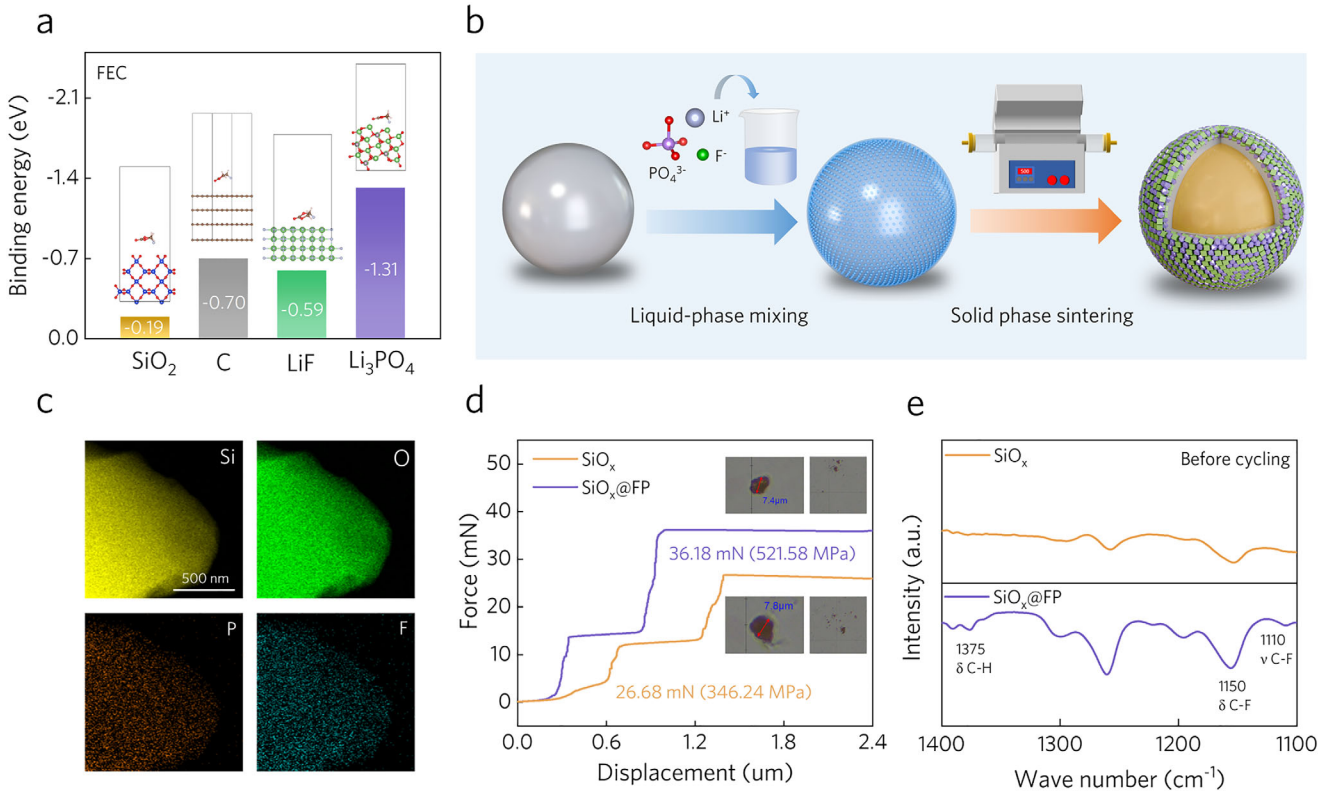


FIGURE 1 | (a) Binding energies between the FEC with SiO_x, C, LiF and Li_3PO_4 surface; (b) Schematic illustration of SiO_x@FP material synthesis; (c) EDS mapping images of SiO_x@FP material; (d) Crushing tests of single particle for SiO_x and SiO_x@FP materials; (e) FTIR spectra of SiO_x and SiO_x@FP surfaces before cycling.

the subsequent characterization (Figure S17). Notably, the more pronounced peaks observed on SiO_x@P further demonstrate the stronger adsorption of FEC on Li_3PO_4 (Figure S18).

2.2 | Regulated Electrochemical Decomposition

The non-faradaic capacitance-potential curves also showed that the potential and capacitance of SiO_x@FP at the potential of zero charge (PZC) both changed compared with that of SiO_x, indicating the different adsorption features in the IHP (Figure S19). According to the calculation results, Li_3PO_4 exhibits selective adsorption toward FEC, thereby facilitating the formation of a FEC-enriched IHP. Next, the FEC distribution within the inner Helmholtz plane of various anodes under static conditions was analyzed using depth-profiling Raman spectroscopy (the schematic setup is shown in Figure S20) [38]. Through tracking the disappearance of the Si Raman peak (~520 cm^{-1}), the solid-liquid interface was identified (Figure S20). As shown in Figure 2a and Figure S21, intensified peaks corresponding to the C–F stretching vibration (~865 cm^{-1}) and ring skeletal deformation of FEC (~906 cm^{-1}) were detected near the interface of SiO_x@FP anode in the FEC solvent, suggesting more FEC molecules are concentrated at the interface. In sharp contrast, the corresponding peaks near the surface of the pristine SiO_x anodes are consistent with those observed in the bulk electrolyte, indicating the absence of FEC accumulation at the interface. These results further confirm that FEC molecules are enriched on the surface of SiO_x@FP due to a stronger adsorption. To further identify the role of Li_3PO_4, the same measurements were conducted on SiO_x@F or SiO_x@P, respectively (Figure S22). Consistent with the expected result, enhanced Raman signals of FEC were observed in the surface of SiO_x@P anode. The Raman signals related to FEC are only intensified on the surface of SiO_x@P anode, further verifying the adsorption effect of Li_3PO_4 toward FEC. Moreover, the similar measurement in the EC/DEC (1/1, v/v) solution showed that the corresponding peaks (~900 cm^{-1}) near the surface of SiO_x@FP anodes are consistent with those in the bulk electrolyte (Figure S23), indicating no preferential adsorption. Combining these experimental observations with binding energy calculations, FEC molecules are found to be selectively adsorbed on the Li_3PO_4 surface (Figure S24). Besides, the SiO_x@FP electrode showed a smaller contact angle with the electrolyte as well as pure FEC solvent than the pristine SiO_x electrode (Figure S25). The enhanced electrolyte wettability can be attributed to the stronger interaction between the Li_3PO_4 and electrolyte components.

Subsequently, in situ FTIR was performed to reveal the evolution of IHP during SEI formation (Figure 2b, Figures S26 and S27). For SiO_x, the peak intensity of EC (~1800 cm^{-1}) and Li^+-EC (~1770 cm^{-1}) reduced obviously while the peak intensity of LEDC (~1580 cm^{-1}) increased, suggesting the excess decomposition of EC solvents upon discharging process. By contrast, the corresponding peaks of EC decomposition and side reaction product are inhibited in the SiO_x@FP anode. In addition, the reduction of FEC (~1835 cm^{-1}) exhibits stronger tendency in the SiO_x@FP, confirming that the preferential adsorption facilitates the accelerated reduction of FEC with the assistance of the

15214095, 0, Downloaded from https://advanced.onlinelibrary.wiley.com/doi/10.1002/adma.74536 by University Town Of Shenzhen, Wiley Online Library on [08/09/2026]. See the Terms and Conditions (https://onlinelibrary.wiley.com/terms-and-conditions) on Wiley Online Library for rules of use; OA articles are governed by the applicable Creative Commons License

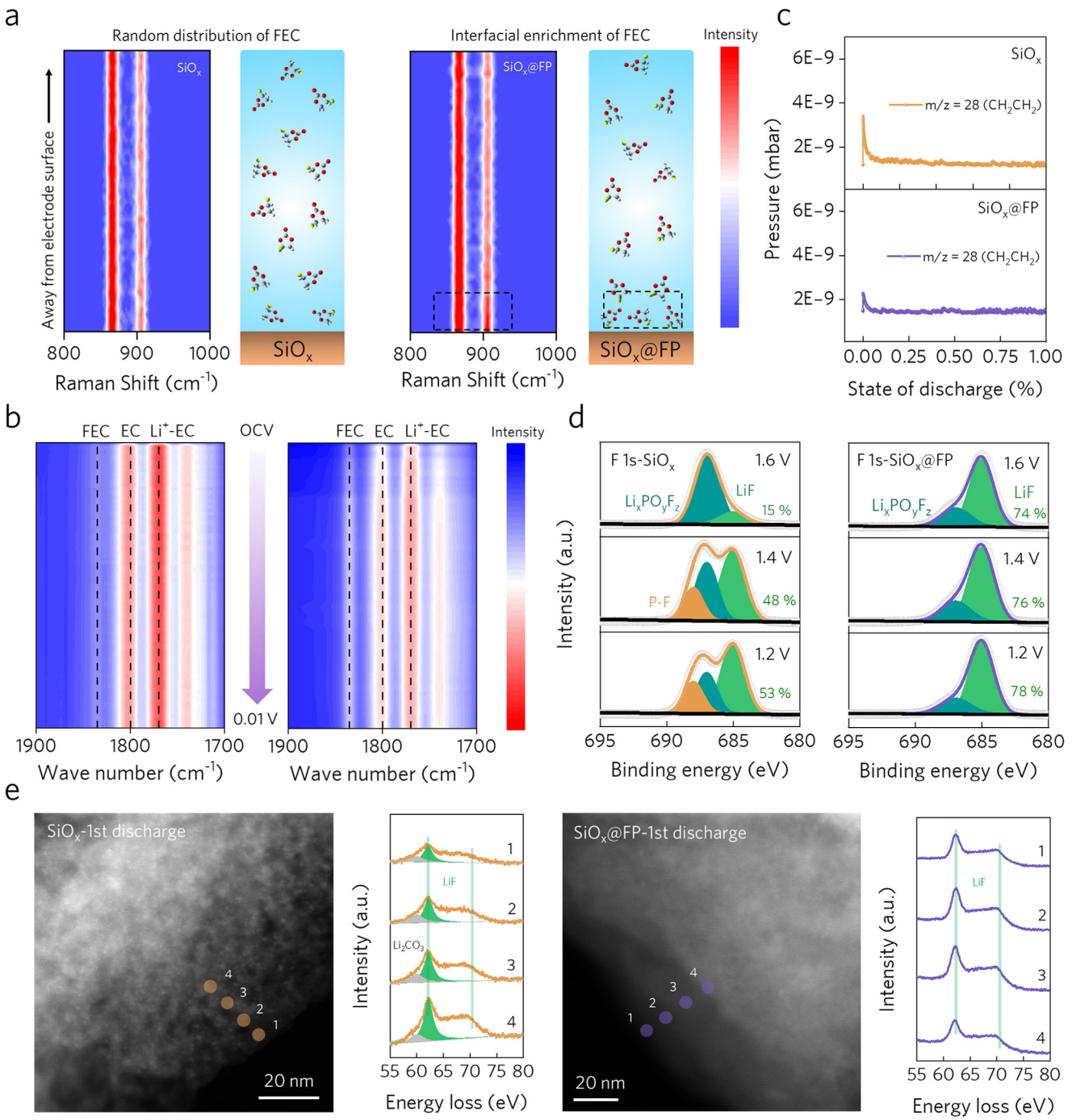


FIGURE 2 | (a) Depth-profiling Raman spectra of SiO_x and SiO_x@FP surfaces in the pure FEC solvent (the test depth is about 0.5 μm and chemical diagrams are FEC); (b) in situ FTIR difference spectra on SiO_x (left) and SiO_x@FP (right) surface during galvanostatic discharging to 0.01 V; (c) ethylene evolution for SiO_x and SiO_x@FP anodes during galvanostatic discharging to 0.01 V; (d) F 1s XPS spectra of SiO_x and SiO_x@FP anodes at the first discharge under different potentials; (e) electron energy loss spectroscopy (EELS) spectra near the surface of SiO_x and SiO_x@FP anodes at the lithiated state.

Li_3PO_4 coating layer, which is consistent with the intensified FEC reduction peak in the cyclic voltammograms (CV) curves (Figure S28). Operando differential electrochemical mass spectrometry (DEMS) was also conducted to monitor the ethylene evolution during SEI formation (Figure 2c) [39]. More ethylene gas was detected in SiO_x system due to the more reduction of EC solvents (Figure S3), which leads to the formation of more unstable organics and Li_2CO_3 species, finally inducing the thickening of SEI layer [27]. Furthermore, the composition evolution of the SEI during the first discharge process was recorded by XPS under different cut-off potentials (Figure 2d). Distinctive and stable LiF peaks can be detected in the SiO_x@FP anodes at the early stages of SEI formation. By contrast, the SEI layer on pristine SiO_x anodes primarily consisted of unfavorable $LiPF_6$ decomposition species (e.g. Li_xPF_z, $Li_xPO_yF_z$). It should be noted that a strong LiF signal was observed on the SiO_x@FP anode before cycling. To further investigate the origin of this signal, the same measurements were conducted on the SiO_x@P anode. By comparing the F 1s XPS

15214095, 0, Downloaded from https://advanced.onlinelibrary.wiley.com/doi/10.1002/adma.74536 by University Town Of Shenzhen, Wiley Online Library on [08/09/2026]. See the Terms and Conditions (https://onlinelibrary.wiley.com/terms-and-conditions) on Wiley Online Library for rules of use; OA articles are governed by the applicable Creative Commons License

spectra of SiO_x and SiO_x@P (Figure S29), it can be clearly seen that the formation rate of LiF in SiO_x@P is much higher than that in SiO_x under the same potential. This result further confirms that the stronger interaction between Li_3PO_4 and FEC molecules promotes the accelerated reduction of FEC. These results indicate that the pre-constructed coating layer not only promotes the decomposition of FEC and its participation in SEI formation but also simultaneously inhibits the decomposition of EC solvent. In situ electrochemical impedance spectroscopy (EIS) measurements during the first cycle (Figure S30) further confirmed that, both the SEI resistance (R_{SEI}) and charge transfer resistance (R_{ct}) of SiO_x@FP anodes rapidly stabilized and remained low values even when upon re-oxidization to 1.5 V, which confirms the formation of an SEI layer with reduced interfacial resistance and enhanced structural robustness. EIS spectra collected after the second cycle also reveal that the SiO_x@FP electrode delivers reduced impedance, further verifying the structural robustness of the as-formed SEI film (Figure S31). The morphology and chemical composition of SEI layer at the first discharge state were further examined using electron energy loss spectroscopy (EELS) spectral imaging (Figure 2e). The peak at 62.2 eV with a sharp shoulder is assigned as LiF and the broad peak centered around 60 eV is ascribed to lithium carbonate [40]. The compact and uniform LiF coating layer was observed from the surface to the inner layer of SiO_x@FP anode. In contrast, the SiO_x anode developed a porous SEI layer rich in Li_2CO_3, consistent with the above results.

2.3 | Electrochemical Performance of SiOx-Based Anodes

The electrochemical performance of SiO_x-based electrodes was first evaluated in half-cells through the galvanostatic cycling tests. The preconstructed stable SEI alleviates the side reactions induced by SEI growth, thereby improving the initial CE (Figure S32). It should be noted that the SiO_x material adopted in this work was not pre-lithiated; the contribution of SEI formation to the initial CE loss is limited. Therefore, further performance optimization relies on ex situ and in situ lithium compensation technologies. After 200 cycles at 0.4 A g^{-1}, a continuous decline of capacity was observed in SiO_x, resulting in a capacity retention of 57% after 200 cycles (Figure S33). By sharp contrast, SiO_x@FP delivered a significantly improved cycling performance, with a reduced capacity decay rate of merely 11%. Combining with results of dQ/dV curves, the peaks of SiO_x@FP remained unchanged in the subsequent cycles, indicating the high reversibility and stability of SEI layer (Figure S33) [41]. At an elevated specific current of 0.8 A g^{-1}, SiO_x@FP exhibited an impressive long-term cycling stability (1086 mAh g^{-1}, corresponding to 81% capacity retention) after 300 cycles with the mass loading of 1.5 mg cm^{-2} (Figure 3a). In sharp contrast, the pristine SiO_x anode exhibits a noticeable drop followed by a gradual rise in the discharge capacity when the current density increases to 0.8 A g^{-1}, which can be attributed to the repeated generation of an unstable and thick SEI layer [3, 42]. Besides, the CE of SiO_x@FP anode is higher and smoother during the long-term cycling process (Figure S34), indicating suppressed side reactions and a more stable interfacial layer on the surface of SiO_x@FP anode. In addition, the cycling stability of SiO_x anodes coated exclusively with LiF or Li_3PO_4 was also evaluated (Figure S35). It can be observed that a pure LiF coating lacks a mechanism to regulate electrochemical decomposition during long-term cycling, whereas a pure Li_3PO_4 coating lacks the high surface energy and electrochemical stability characteristic of LiF, resulting in inferior electrochemical performance compared to the mixed coating. The synergistic action of LiF and Li_3PO_4 is crucial for forming a stable interface. Furthermore, even under a high mass loading (~4.5 mg cm^{-2}), SiO_x@FP still showed a reversible capacity of 1259 mAh g^{-1} after 100 cycles (Figure 3b). The structural transformation of the pristine SiO_x anode and SiO_x@FP anode were further characterized by in situ Raman spectra [43, 44]. The characteristic peak of Si is located at approximately 520 cm^{-1}. As shown in Figure S36, the intensity of vibration peaks attenuated significantly for the pristine SiO_x anode during the delithiation process, suggesting the formation of numerous inactive Si. By contrast, the Raman spectra of SiO_x@FP anode exhibit the high reversibility.

In order to probe the origin of enhanced cycling stability, in situ expansion ratio measurements were performed in an electrochemical dilatometer cell. To ensure that the overall volume change of cells is mainly determined by anodes, $LiFePO_4$ cathode was selected due to its excellent structural stability. The swelling ratio curves of SiO_x showed a large initial irreversible volume expansion (~19%) and gradually became increasingly pronounced, indicating uncontrolled SEI growth (Figure 3c). In comparison, SiO_x@FP electrode not only exhibited a lower expansion rate but also demonstrated better reversibility of volume variations than SiO_x, which can be attributed to a more resilient SEI. The cross-sectional SEM images of anodes after 200 cycles (Figure S37) also showed that the SiO_x@FP electrode exhibited a much lower thickness variation (~21%) than that of SiO_x electrode (~61%) after 200 cycles. The above findings are consistent with the EIS results after cycling (Figure 3d and Figure S38). For pristine SiO_x, the significantly increased R_{SEI} and R_{ct} may result from the excessive decomposition of the electrolyte, leading to the overgrowth of SEI; whereas SiO_x@FP delivered lower values of R_{SEI} (12.1 Ω) and R_{ct} (25.5 Ω) after 200 cycles, exhibiting better stability.

The impact of different SEI on the reaction kinetics of SiO_x and SiO_x@FP anodes was further evaluated by stepped sweep rate CV tests (Figure S39). Based on the Randles-Sevcik equation [18], the apparent diffusion coefficient of Li^+ (D_{Li}) of SiO_x@FP was calculated to be 4.13×10^{-9} cm^2 s^{-1}, which is higher than that (2.98×10^{-9} cm^2 s^{-1}) of SiO_x. As a result, the SiO_x@FP anode demonstrated superior rate performance (~1010 mAh g^{-1} at 2.4 A g^{-1}) over pristine SiO_x (Figure 3e and Figure S40). These results verify the remarkable improvements of interfacial stability and electrode kinetics with the help of a robust SEI layer. The capacity retention and rate performance of SiO_x@FP anodes were compared with those of recently reported surface-modified SiO_x-based materials (Figure 3f). Under comparable testing conditions, the present work demonstrates state-of-the-art electrochemical performance (Table S1). Subsequently, full coin cells were assembled and tested to evaluate the practical applicability of the proposed material (Figure S41), and full cells incorporating the SiO_x@FP anode delivered the significantly enhanced cycling stability. To evaluate the practical value of this interfacial reconstruction strategy, Ah-level $LiNi_{0.8}Co_{0.1}Mn_{0.1}O_2$||graphite-$SiO_x$@FP pouch cells were assembled and tested between 2.5 and

15214095, 0, Downloaded from https://advanced.onlinelibrary.wiley.com/doi/10.1002/adma.74536 by University Town Of Shenzhen, Wiley Online Library on [08/09/2026]. See the Terms and Conditions (https://onlinelibrary.wiley.com/terms-and-conditions) on Wiley Online Library for rules of use; OA articles are governed by the applicable Creative Commons License

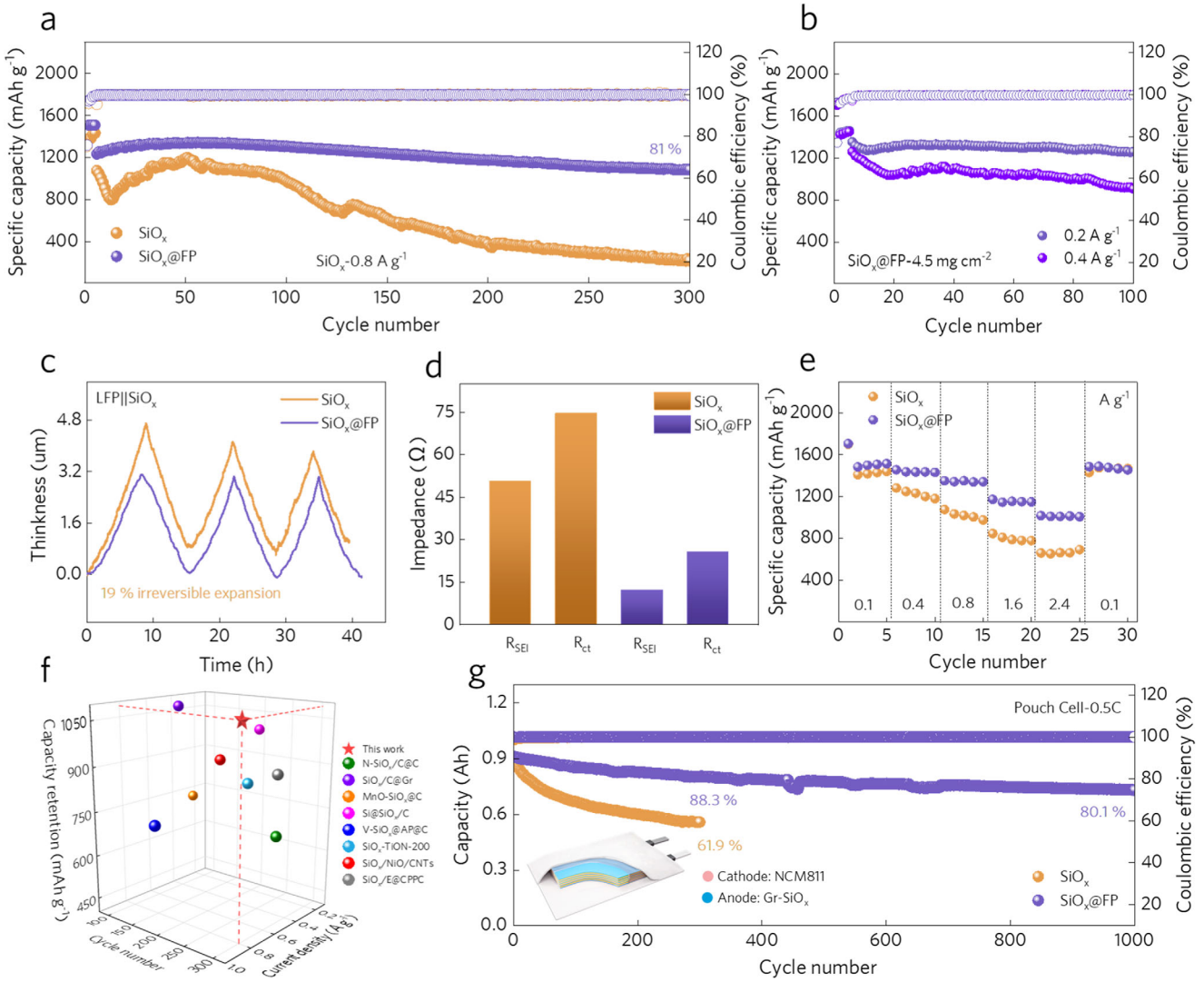


FIGURE 3 | (a) Galvanostatic cycling performance and CE of various SiO_x anodes at a current density of 0.1 A g^{-1} for the first 5 cycles and 0.8 A g^{-1} for the subsequent cycles; (b) galvanostatic cycling performance and CE of SiO_x@FP anodes with high mass loading; (c) in situ expansion ratio measurements of LFP||SiO_x cells; (d) resistance (R_{SEI} and R_{ct}) of various half cells calculated from the simulation of the EIS; (e) rate performance of SiO_x and SiO_x@FP anodes; (f) comparison of SiO_x-based anodes electrochemical performance through interfacial modification (all data are taken from the original publications and details are provided); (g) galvanostatic cycling performance and CE of pouch cells at a rate of 0.5C with various graphite-SiO_x anodes.

4.2 V (Figure 3g, Figure S42, and Table S2), which contain 30 wt.% SiO_x materials in the anodes. The SiO_x@FP-based cell operated normally after 1000 cycles with an average CE of 99.96%, exhibiting superior performance compared with recent studies (Table S3). Furthermore, a pouch cell with a lower FEC content was also tested, demonstrating similarly excellent cycling stability (Figure S43). By achieving the efficient utilization of FEC, the strategy proposed in this work offers valuable insights for the development of more cost-effective (Table S4) and environmentally friendly electrolyte designs.

2.4 | Composition and Structural Characterization of SEI Layer

Next, the chemical compositions of SEI layers were analyzed using XPS and sXAS to reveal the interface evolution of the SiO_x-based anode. During the initial cycles, both C 1s and P 2p XPS spectra of SiO_x exhibited stronger $-CO_3$ and P–F signals, which align with the conclusions derived from the calculations and in situ FTIR spectra (Figure S44). After 200 cycles, the continuously growing SEI on the SiO_x anode leads to an undesirable composition primarily consisting of Li_2CO_3, Li_xPF_y and $Li_xPO_yF_z$ (Figure 4a and Figure S45). In stark contrast, a bilayer SEI comprising organics and LiF–Li_3PO_4 compounds, arranged hierarchically from the outer to the inner layer, was formed on SiO_x@FP. The results of sXAS with total electron yield (TEY) mode (Figure S46) further confirm that there are more Li_2CO_3, lithium carboxylate, and P-F containing species generated on the SiO_x surface compared with that of SiO_x@FP, which derived from the decomposition of EC and $LiPF_6$. Therefore, the introduction of a multifunctional LiF–Li_3PO_4 layer effectively passivates the surface and mitigates excessive electrolyte decomposition.

15214095, 0, Downloaded from https://advanced.onlinelibrary.wiley.com/doi/10.1002/adma.74536 by University Town Of Shenzhen, Wiley Online Library on [08/09/2026]. See the Terms and Conditions (https://onlinelibrary.wiley.com/terms-and-conditions) on Wiley Online Library for rules of use; OA articles are governed by the applicable Creative Commons License

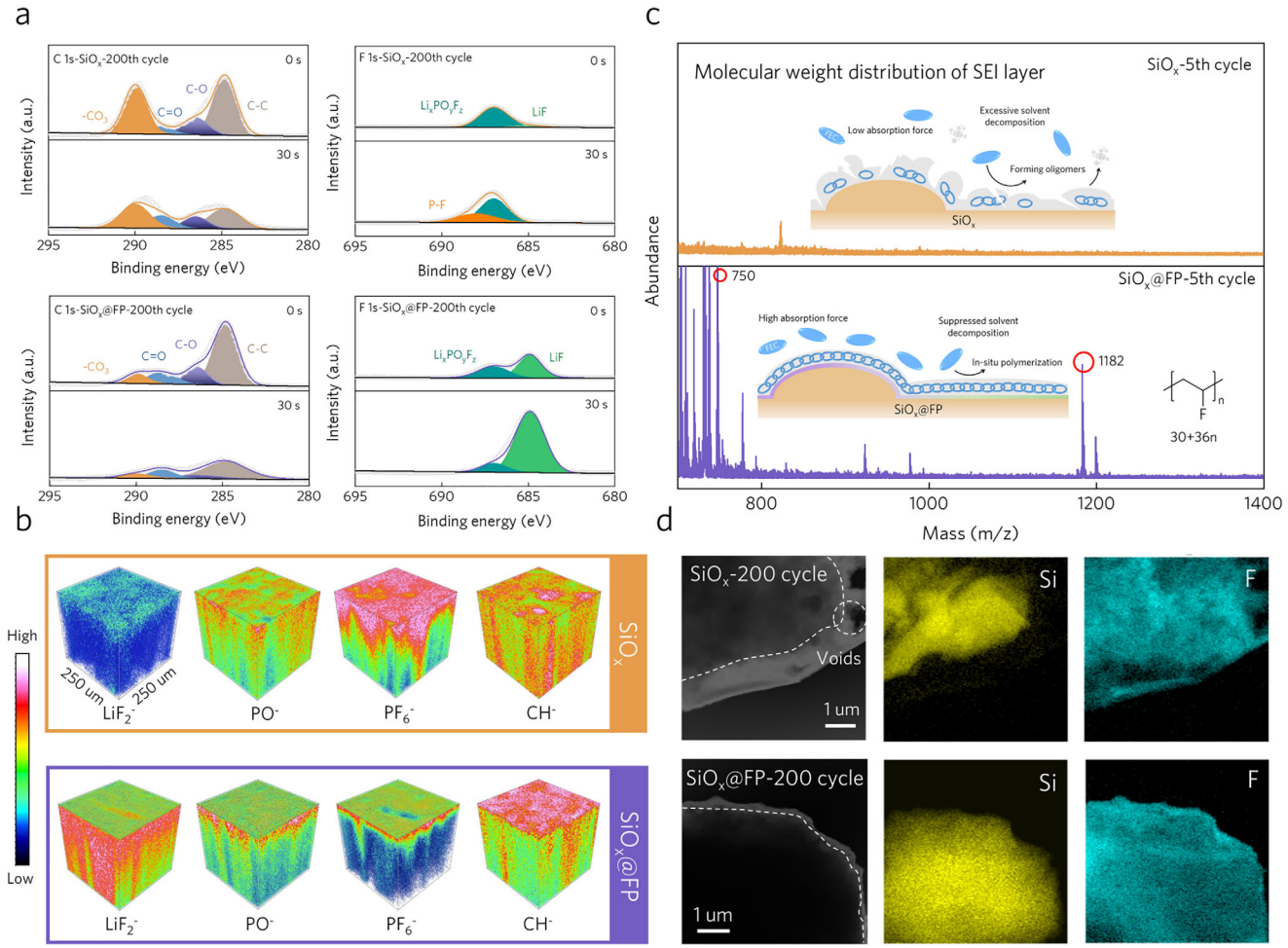


FIGURE 4 | (a) C 1s and F 1s XPS spectra of various SiO_x anodes after 200 cycles at 0.4 A g^{-1}; (b) ToF-SIMS three-dimensional distributions of SiO_x and SiO_x@FP anodes after 200 cycles at 0.4 A g^{-1} (the higher color saturation representing the higher content); (c) MALDI-ToF-MS spectra of SEI on the SiO_x and SiO_x@FP anodes; (d) Cryo-HRTEM images of SiO_x and SiO_x@FP anodes after 200 cycles at 0.4 A g^{-1} and corresponding EDS mapping images.

To further explore the spatial distribution of various components within SEI, time of flight secondary-ion mass spectroscopy (ToF-SIMS) measurements were carried out on cycled anodes (Figures 4b and S47). The intense PF_6^- and CH^- signals, corresponding to reduction products of $LiPF_6$ and electrolyte solvents, respectively, were observed in the SiO_x anode. Combined with the depth profiles, these signals revealed a disordered distribution, further confirming uncontrolled electrolyte decomposition during cycling [45]. For SiO_x@FP, PF_6^- and CH^- signals are confined within a thin layer in the outermost 3D-rendering space, leaving the inner region predominantly occupied by LiF and Li_3PO_4. This distribution aligns closely with the XPS results and reflects the characteristic of an ideal SEI for SiO_x anodes [46]. The polymer fragments of the SEI layer were further detected by matrix-assisted laser desorption/ionization time-of-flight mass spectrometry (MALDI-ToF-MS) [47]. As shown in Figures 4c and S48, the peaks appearing in the higher mass region were found on the interphase of SiO_x@FP anode. A few obvious polyvinyl fluoride (–$[CH_2$–$CHF]_{n}$–) signals were observed at 750 and 1182 Da (corresponding to $n = 20$ or 32, respectively) on the SiO_x@FP surface, indicating the polymerization of FEC-derived fluoroethylene (Figure S3). These organic SEI components with higher molecular masses generally exhibit superior mechanical properties and enhanced dissolution resistance to better preserve the SEI structure. As shown in the MALDI-ToF-MS results of SiO_x@FP after 200 cycles (Figure S49), distinct signals of polymerized species persist, indicating their high robustness in accommodating volume variation. By contrast, only low-mass species as decomposition organic products were detected on the surface of pristine SiO_x anodes, which are insufficient to tolerate the large volume swings. It should be noted that the organic outer layer of the SiO_x@FP anode shows a higher degree of polymerization, rather than a higher overall organic content. Taken together with the EIS results (Figures S30 and S38), the polymerization of FEC-derived species leads to the formation of a compact and thin SEI that mitigates electrolyte swelling and shortens ion transport pathways, thereby preserving efficient ionic conductivity within SEI. In addition, the inner Li_3PO_4 layer with relatively high ionic conductivity reduces interfacial impedance and promotes charge-transfer kinetics. To further elucidate the respective roles of LiF and Li_3PO_4 in regulating interfacial reactions, MALDI-ToF-MS measurements were performed on SiO_x@F and SiO_x@P anodes (Figure S50). While characteristic polyvinyl fluoride signals were detectable on the SiO_x@P anode, the SEI formed on the SiO_x@F

15214095, 0, Downloaded from https://advanced.onlinelibrary.wiley.com/doi/10.1002/adma.74536 by University Town Of Shenzhen, Wiley Online Library on [08/09/2026]. See the Terms and Conditions (https://onlinelibrary.wiley.com/terms-and-conditions) on Wiley Online Library for rules of use; OA articles are governed by the applicable Creative Commons License

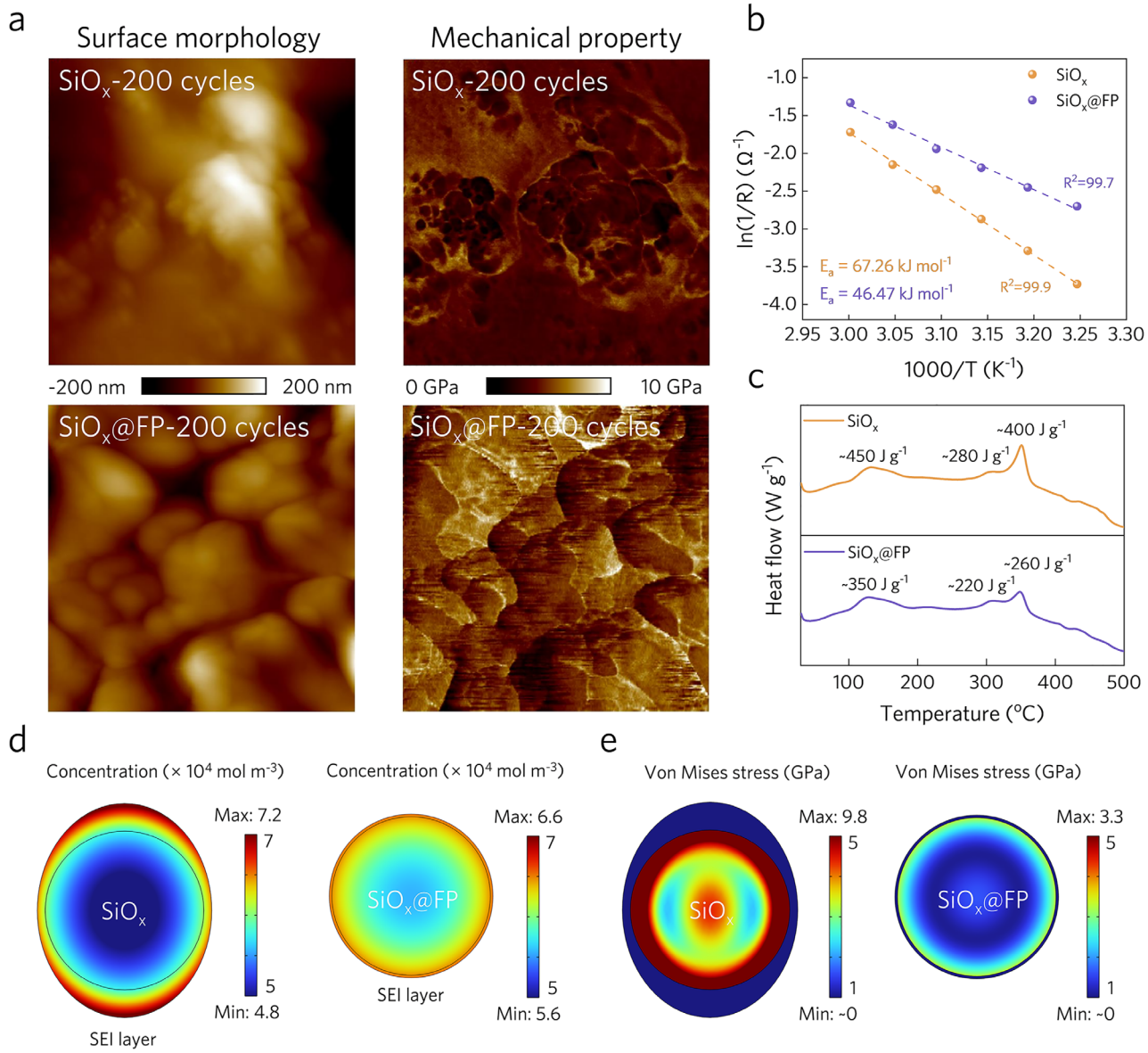


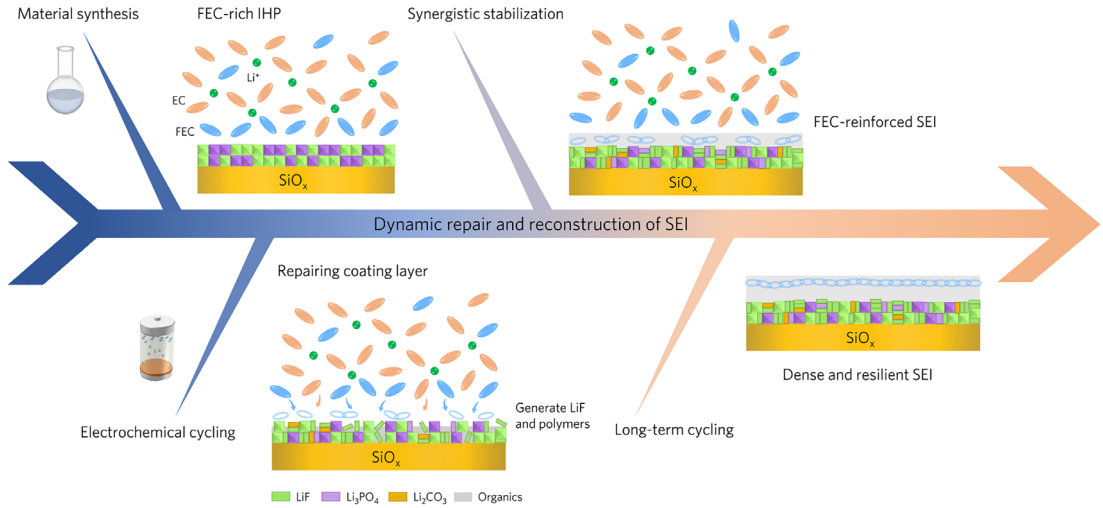
FIGURE 5 | (a) Surface morphology (left) and mechanical property (right) of SEI on the SiO_x and SiO_x@FP anodes after 200 cycles measured via AFM (2.5 μm × 2.5 μm); (b) activation energy of the Li^+ penetrating through SEI by Arrhenius analysis; (c) DSC curves of SiO_x and SiO_x@FP anodes, recorded ex situ after the electrode underwent five initial cycles and subsequent galvanostatic lithiation to 0.01 V; (d, e) FEM simulation of SiO_x particle and SiO_x@FP particle with different SEI layer.

anode was dominated by low-molecular-weight species, indicating limited polymerization in the absence of Li_3PO_4-mediated FEC enrichment.

The above results suggest that enhancing the interfacial concentration of reactive monomers via preferential adsorption effectively increases their surface activity, thereby promoting electrochemically induced polymerization at the electrode-electrolyte interface. Such surface enrichment not only facilitates interfacial electron transfer and radical coupling under confinement [48] but also increases the local availability of monomers for radical-monomer interactions, reducing the likelihood of premature chain termination or chain-transfer events and enabling sustained chain propagation [49, 50]. Consequently, the formation of higher-molecular-weight organic species on the SiO_x@FP surface can be attributed to the enrichment of FEC molecules within the IHP, which promotes their interfacial decomposition and drives an aggregation-facilitated polymerization pathway (Figure 4c).

In addition to the composition, the uniformity and microstructure of different SEIs were further examined. The cryogenic high-resolution transmission electron microscopy (cryo-HRTEM) images (Figure 4d and Figure S51) reveal a loose, thick and damaged SEI layer covered on the SiO_x particle, characterized by uneven element distribution and voids due to the repeated SEI disruption and reconstruction. In contrast, a homogeneous distribution of F element can be observed on the surface of SiO_x@FP anode after long-term cycling, indicating the formation of a robust and LiF-rich SEI layer. Fast Fourier transformation (FFT) of cryo-HRTEM images (Figure S52) shows that the uneven SEI of SiO_x is composed solely of amorphous species. In contrast, the uniform and thin (~20 nm) SEI on SiO_x@FP consists

15214095, 0, Downloaded from https://advanced.onlinelibrary.wiley.com/doi/10.1002/adma.74536 by University Town Of Shenzhen, Wiley Online Library on [08/09/2026]. See the Terms and Conditions (https://onlinelibrary.wiley.com/terms-and-conditions) on Wiley Online Library for rules of use; OA articles are governed by the applicable Creative Commons License



SCHEME 2 | Schematic illustration of the dynamic repair mechanism enabled by the LiF–Li_3PO_4 coating on the SiO_x anode.

of amorphous organic components embedded with abundant inorganic species, including LiF and Li_3PO_4. To conclude, the pre-synthesized coating layer contributes to construct a thin and robust SEI layer with abundant and uniform LiF–Li_3PO_4 inner layer and organic outer layer with higher molecular weight, which can restrain the excess electrolyte decomposition and the repeated SEI growth. As confirmed by the SEM images (Figure S53), the SiO_x@FP electrode still maintains a relatively stable and uniform structure after cycling, whereas the SiO_x electrode exhibits pronounced swelling and the formation of pores due to the excessive growth of SEI layer [3, 51].

2.5 | Physicochemical Properties of SEI Layer

To explore the intrinsic relationship between the structure of SEI and its electrochemical performance, the physicochemical properties of SEIs were investigated. First, atomic force microscopy (AFM) was performed to evaluate the mechanical properties of SEI of SiO_x and SiO_x@FP anodes (Figure 5a). Compared with the SEI on the SiO_x surface, which exhibits a distinct bulging morphology, the SEI on the SiO_x@FP anode shows a smooth surface, in line with the cryo-HRTEM results. Accordingly, the corresponding Derjaguin-Müller-Toporov (DMT) modulus of SEI in SiO_x@FP anode (5.04 GPa) is much higher than that (3.63 GPa) of SEI in SiO_x anode (Figure S54), which is not only attributed to the outer layer of high-molecular-weight organic species, but also originating from the contribution of a mechanically robust inner inorganic layer. By contrast, the lower DMT modulus of SiO_x can be ascribed to a loosely packed SEI structure resulting from the disordered intermixing of low-molecular-weight organic species with inorganic components. It is worth noting that an SEI layer with a high DMT modulus could alleviate the stress caused by volume expansion.

The activation energy (E_a) for Li^+ transport through the SEI layer was calculated using the Arrhenius equation based on the R_{SEI} values obtained at various temperatures (Figure 5b and Figure S55). The value of E_a for SiO_x@FP (46.7 kJ mol^{-1}) is much lower than that for the pristine SiO_x (67.3 kJ mol^{-1}), indicating enhanced Li^+ migration kinetics, which helps to relieve the anisotropy expansion of Si-based materials [52]. Next, differential scanning calorimeter (DSC) measurement of fully lithiated SiO_x anodes was employed to analyze the thermal stability of SEI layer (Figure 5c). The total heat-releasing of SiO_x anode (~1130 J g^{-1}) is higher than that of SiO_x@FP anode (~830 J g^{-1}), indicating the formation of a thick SEI layer rich in short-chain organics forms on the former, consistent with cryo-HRTEM observations.

In order to provide a vivid demonstration, Li^+ concentration and stress distribution of active material particles with different SEI layers were simulated through the finite element method (FEM) in Figure 5d,e [53]. The related parameter settings were measured by experiments. For SiO_x@FP particles, Li^+ appears at a lower concentration in the SEI layer and a homogeneous distribution in the whole, suggesting the high-efficiency Li^+ diffusion driven by the superior SEI layer. At the same time, the superior SEI layer provides a better mechanical confinement effect to resist the expansion of the particle and achieves a uniform distribution of stress (Max: 3.3 GPa). By contrast, a high concentration of Li^+ accumulates on the uneven SEI layer for SiO_x system. Hence, the heterogeneity of Li^+ transport and poor mechanical properties of SEI result in higher stress in the SiO_x particles (Max: 9.8 GPa), which gives rise to structural failure and performance degeneration of the electrode.

3 | Conclusion

In summary, we developed a dynamic interphase modification strategy to construct a durable SEI layer for SiO_x anodes by synergistically coupling chemical coating with in situ regulated electrolyte decomposition, where LiF serves as a framework of SEI growth and stabilize the SEI inner structure due to its wide band gap and high interfacial energy, while Li_3PO_4 directs the subsequent SEI growth by enhancing the utilization of FEC, including the repair of inorganic inner layer with LiF and the formation of the high-molecular-weight organic outer layer (Scheme 2). The proposed mechanism delivers critical insights for the better utilization of well-established FEC additives in the industry. The electrochemically formed SEI components mitigate structural damage and help maintain SEI integrity under severe

15214095, 0, Downloaded from https://advanced.onlinelibrary.wiley.com/doi/10.1002/adma.74536 by University Town Of Shenzhen, Wiley Online Library on [08/09/2026]. See the Terms and Conditions (https://onlinelibrary.wiley.com/terms-and-conditions) on Wiley Online Library for rules of use; OA articles are governed by the applicable Creative Commons License

volume swings. Combined with the multiple experimental characterizations and theoretical calculation, we demonstrate that the resultant SEI comprising an inorganic-rich inner layer and an elastic organic outer layer effectively accommodates the volume change of SiO_x and suppresses excessive electrolyte decomposition. This ultimately leads to record-high electrochemical performance of SiO_x anodes. This proposed SEI design principle, which balances uniformity and long-term stability, provides a fresh insight into interfacial engineering for high-energy-density anodes with pronounced volume changes. Based on the design strategy proposed in this work, more suitable coating layers can be screened in future research from two perspectives: mechanical and chemical stability, as well as interfacial interaction with electrolyte components.

Acknowledgements

This work was financially supported by the National Natural Science Foundation of China (No. 52303263) and the Shenzhen Science and Technology Research Grant (No. ZDSYS201707281026184). The authors thank the support from the XMCD beamline (BL12B) in the National Synchrotron Radiation Laboratory (NSRL).

Conflicts of Interest

The authors declare no conflicts of interest.

Data Availability Statement

The data that support the findings of this study are available from the corresponding author upon reasonable request.

References

1. J. B. Goodenough and Y. Kim, "Challenges for Rechargeable Li Batteries," *Chemistry of Materials* 22 (2009): 587–603, https://doi.org/10.1021/cm901452z.

2. Z. Liu, Q. Yu, Y. Zhao, et al., "Silicon Oxides: A Promising Family of Anode Materials for Lithium-Ion Batteries," *Chemical Society Reviews* 48 (2019): 285–309, https://doi.org/10.1039/C8CS00441B.

3. G. Qian, Y. Li, H. Chen, et al., "Revealing the Aging Process of Solid Electrolyte Interphase on SiOx Anode," *Nature Communications* 14 (2023): 6048, https://doi.org/10.1038/s41467-023-41867-6.

4. R. Wu, X. Du, T. Liu, et al., "Robust and Fast-Ion Conducting Interphase Empowering SiO x Anode Toward High Energy Lithium–Ion Batteries," *Advanced Energy Materials* 14 (2023): 2302899, https://doi.org/10.1002/aenm.202302899.

5. M. Khan, S. Yan, M. Ali, et al., "Innovative Solutions for High-Performance Silicon Anodes in Lithium-Ion Batteries: Overcoming Challenges and Real-World Applications," *Nano-Micro Letters* 16 (2024): 179, https://doi.org/10.1007/s40820-024-01388-3.

6. X. Zhuang, S. Zhang, Z. Cui, et al., "Interphase Regulation by Multifunctional Additive Empowering High Energy Lithium-Ion Batteries With Enhanced Cycle Life and Thermal Safety," *Angewandte Chemie International Edition* 136 (2023): 202315710, https://doi.org/10.1002/ange.202315710.

7. Y. Zhou, X. Fang, B. Li, et al., "Mechanically Robust Bilayer Solid Electrolyte Interphase Enabled by Sequential Decomposition Mechanism for High-Performance Micron-Sized SiO x Anodes," *Angewandte Chemie International Edition* 64 (2025): 202514076, https://doi.org/10.1002/anie.202514076.

8. X. Chen, W. R. Li, C. Z. Luo, et al., "A Bioinspired Piezoelectric Stress Buffer Layer for SiO x -Based Electrodes Toward High-Energy Lithium Batteries," *Advanced Materials* 27 (2025): 04360, https://doi.org/10.1002/adma.202504360.

9. J. Chen, X. Fan, Q. Li, et al., "Electrolyte Design for LiF-Rich Solid–Electrolyte Interfaces to Enable High-Performance Microsized Alloy Anodes for Batteries," *Nature Energy* 5 (2020): 386–397, https://doi.org/10.1038/s41560-020-0601-1.

10. J. Lin, L. Wang, Q. Xie, et al., "Stainless Steel-Like Passivation Inspires Persistent Silicon Anodes for Lithium-Ion Batteries," *Angewandte Chemie International Edition* 62 (2023): 202216557, https://doi.org/10.1002/anie.202216557.

11. C. Wang, Y. Xie, Y. Huang, et al., "Li 3 PO 4 -Enriched SEI on Graphite Anode Boosts Li + De-Solvation Enabling Fast-Charging and Low-Temperature Lithium-Ion Batteries," *Angewandte Chemie International Edition* 63 (2024): 202402301, https://doi.org/10.1002/anie.202402301.

12. G. M. Hobold, C. Wang, K. Steinberg, Y. Li, and B. M. Gallant, "High Lithium Oxide Prevalence in the Lithium Solid–Electrolyte Interphase for High Coulombic Efficiency," *Nature Energy* 9 (2024): 580–591, https://doi.org/10.1038/s41560-024-01494-x.

13. D. Z. Grabco, K. M. Pyrtsac, and O. A. Shikimaka, "Mechanical Properties of Polycrystalline Copper and Single-Crystal LiF initial Components for Composite System Cu/LiF," *Surface Engineering and Applied Electrochemistry* 52 (2016): 233–241, https://doi.org/10.3103/S1068375516030066.

14. X. Fan, X. Ji, F. Han, et al., "Fluorinated Solid Electrolyte Interphase Enables Highly Reversible Solid-State Li Metal Battery," *Science Advances* 4 (2018): aau9245, https://doi.org/10.1126/sciadv.aau9245.

15. A. Jain, S. P. Ong, G. Hautier, et al., "Commentary: The Materials Project: A Materials Genome Approach to Accelerating Materials Innovation," *APL Materials* 1 (2013): 011002, https://doi.org/10.1063/1.4812323.

16. S. Chen, G. Zheng, X. Yao, et al., "Constructing Matching Cathode–Anode Interphases With Improved Chemo-Mechanical Stability for High-Energy Batteries," *ACS Nano* 18 (2024): 6600–6611, https://doi.org/10.1021/acsnano.3c12823.

17. Y. Yang, Z. Yang, Z. Li, J. Wang, X. He, and H. Zhao, "Rational Electrolyte Design for Interfacial Chemistry Modulation to Enable Long-Term Cycling Si Anode," *Advanced Energy Materials* 13 (2023): 2302068, https://doi.org/10.1002/aenm.202302068.

18. Y. Zhai, Z. Zhong, N. Kuang, et al., "Both Resilience and Adhesivity Define Solid Electrolyte Interphases for a High Performance Anode," *Journal of the American Chemical Society* 146 (2024): 15209–15218, https://doi.org/10.1021/jacs.4c02115.

19. S. Pan, J. Han, Y. Wang, et al., "Integrating SEI Into Layered Conductive Polymer Coatings for Ultrastable Silicon Anodes," *Advanced Materials* 34 (2022): 2203617, https://doi.org/10.1002/adma.202203617.

20. W. An, B. Gao, S. Mei, et al., "Scalable Synthesis of Ant-Nest-Like Bulk Porous Silicon for High-Performance Lithium-Ion Battery Anodes," *Nature Communications* 10 (2019): 1447, https://doi.org/10.1038/s41467-019-09510-5.

21. S. Chen, Z. Deng, J. Li, et al., "Tuning Reaction Kinetics of Fluorinated Molecules to Construct Robust Solid Electrolyte Interphases on SiO x Anode," *Angewandte Chemie International Edition* 64 (2025): 202413927, https://doi.org/10.1002/anie.202413927.

22. K. Xu, "Electrolytes and Interphases in Li-Ion Batteries and Beyond," *Chemical Reviews* 114 (2014): 11503–11618, https://doi.org/10.1021/cr500003w.

23. W. Huang, Y. Wang, L. Lv, et al., "Prefabrication of "Trinity" Functional Binary Layers on a Silicon Surface to Develop High-Performance Lithium-Ion Batteries," *ACS Nano* 17 (2023): 2669–2678, https://doi.org/10.1021/acsnano.2c10698.

24. S. Ma, J. Zhao, H. Xiao, et al., "Modulating the Inner Helmholtz Plane Towards Stable Solid Electrolyte Interphase by Anion-π Interactions for High-Performance Anode-Free Lithium Metal Batteries," *Angewandte*

15214095, 0, Downloaded from https://advanced.onlinelibrary.wiley.com/doi/10.1002/adma.74536 by University Town Of Shenzhen, Wiley Online Library on [08/09/2026]. See the Terms and Conditions (https://onlinelibrary.wiley.com/terms-and-conditions) on Wiley Online Library for rules of use; OA articles are governed by the applicable Creative Commons License

Chemie International Edition 64 (2024): 202412955, https://doi.org/10.1002/anie.202412955.

25. J. Wang, C. Wu, Y. Wu, S. Wang, W. Wang, and X. Hu, "Zwitterion-Induced Interfacial-Potential Regulation Stabilizes Micron-Sized Silicon Anodes in Quasi-Solid-State Lithium-Ion Batteries," *Angewandte Chemie International Edition* 65 (2025): 22965, https://doi.org/10.1002/anie.202522965.

26. Y. Yan, S. Weng, A. Fu, et al., "Tailoring Electrolyte Dehydrogenation With Trace Additives: Stabilizing the LiCoO 2 Cathode Beyond 4.6 V," *ACS Energy Letters* 7 (2022): 2677–2684, https://doi.org/10.1021/acsenergylett.2c01433.

27. M. B. Jassar, C. Michel, S. Abada, et al., "A Perspective on the Molecular Modeling of Electrolyte Decomposition Reactions for Solid Electrolyte Interphase Growth in Lithium-Ion Batteries," *Advanced Functional Materials* 34 (2024): 2313188, https://doi.org/10.1002/adfm.202313188.

28. H. Nakai, T. Kubota, A. Kita, and A. Kawashima, "Investigation of the Solid Electrolyte Interphase Formed by Fluoroethylene Carbonate on Si Electrodes," *Journal of the Electrochemical Society* 158 (2011): A798–A801, https://doi.org/10.1149/1.3589300.

29. X. Chen, X. Li, D. Mei, et al., "Reduction Mechanism of Fluoroethylene Carbonate for Stable Solid–Electrolyte Interphase Film on Silicon Anode," *ChemSusChem* 7 (2014): 549–554, https://doi.org/10.1002/cssc.201300770.

30. C. Xu, F. Lindgren, B. Philippe, et al., "Improved Performance of the Silicon Anode for Li-Ion Batteries: Understanding the Surface Modification Mechanism of Fluoroethylene Carbonate as an Effective Electrolyte Additive," *Chemistry of Materials* 27 (2015): 2591–2599, https://doi.org/10.1021/acs.chemmater.5b00339.

31. X. Liu, Y. Gong, Y. Sun, Z. Xu, and Y. Wang, "Substituent Effect on the Reductive Decomposition Thermodynamics and Kinetics of PFA Ethylene Carbonates for Facilitating SEI Formation of LIB," *Computational and Theoretical Chemistry* 1215 (2022): 113812, https://doi.org/10.1016/j.comptc.2022.113812.

32. C. R. Lee, H. Y. Jang, H. J. Leem, et al., "Surface Work Function-Induced Thermally Vulnerable Solid Electrolyte Interphase Formation on the Negative Electrode for Lithium-Ion Batteries," *Advanced Energy Materials* 14 (2023): 2302906, https://doi.org/10.1002/aenm.202302906.

33. J. Wang, Z. Yang, B. Mao, Y. Wang, Y. Jiang, and M. Cao, "Transgenic Engineering on Silicon Surfaces Enables Robust Interface Chemistry," *ACS Energy Letters* 7 (2022): 2781–2791, https://doi.org/10.1021/acsenergylett.2c01202.

34. L. C. Colocho Hurtarte, H. C. Santana Amorim, J. Kruse, J. Criginski Cezar, W. Klysubun, and J. Prietzel, "A Novel Approach for the Quantification of Different Inorganic and Organic Phosphorus Compounds in Environmental Samples by P L 2,3 -Edge X-Ray Absorption Near-Edge Structure (XANES) Spectroscopy," *Environmental Science & Technology* 54 (2020): 2812–2820, https://doi.org/10.1021/acs.est.9b07018.

35. J. E. N. Swallow, M. W. Fraser, N. H. Kneusels, et al., "Revealing Solid Electrolyte Interphase Formation Through Interface-Sensitive Operando X-Ray Absorption Spectroscopy," *Nature Communications* 13 (2022): 6070, https://doi.org/10.1038/s41467-022-33691-1.

36. F. Wu, Y. Dong, Y. Su, et al., "Benchmarking the Effect of Particle Size on Silicon Anode Materials for Lithium-Ion Batteries," *Small* 19 (2023): 2301301.

37. K. Cheng, S. Tu, B. Zhang, et al., "Material–Electrolyte Interfacial Interaction Enabling the Formation of an Inorganic-Rich Solid Electrolyte Interphase for Fast-Charging Si-Based Lithium-Ion Batteries," *Energy & Environmental Science* 17 (2024): 2631–2641, https://doi.org/10.1039/D4EE00407H.

38. X. Yao, S. Chen, H. Zhu, et al., "Revealing Rate-Determining Factors of Interfacial Lithium-Ion Transport for Efficient Membrane Lithium Separation," *Advanced Functional Materials* 35 (2025): 2426072, https://doi.org/10.1002/adfm.202426072.

39. E. J. McShane, H. K. Bergstrom, P. J. Weddle, D. E. Brown, A. M. Colclasure, and B. D. McCloskey, "Quantifying Graphite Solid-Electrolyte Interphase Chemistry and its Impact on Fast Charging," *ACS Energy Letters* 7 (2022): 2734–2744, https://doi.org/10.1021/acsenergylett.2c01059.

40. X. Zhang, Z. Guo, X. Li, et al., "Cryo-Ultramicrotomy Enables TEM Characterization of Global Lithium/Polymer Interfaces," *Energy & Environmental Science* 17 (2024): 1436–1447, https://doi.org/10.1039/D3EE04189A.

41. Z. You, C. Lin, P. Zheng, et al., "Fluorine-Doping Carbon-Modified Si/SiOx to Effectively Achieve High-Performance Anode," *Small* 21 (2025): 2407215.

42. H. Wang, H. Zhang, L. Wang, et al., "Mediating Solid Electrolyte Interphase Formation Kinetics on SiO x Anodes Using Proton Acceptors," *Angewandte Chemie International Edition* 64 (2025): 202505832, https://doi.org/10.1002/anie.202505832.

43. W. Yan, S. Ma, Y. Su, et al., ""Shooting Three Birds With One Stone": Bi-Conductive and Robust Binder Enabling Low-Cost Micro-Silicon Anodes for High-Rate and Long-Cycling Operation," *Energy Storage Materials* 76 (2025): 104140.

44. J. Peng, R. Shao, S. Huang, et al., "An Interface-Enhanced Continuous 2D-Carbon Network Enabling High-Performance Si Anodes for Li-Ion Batteries," *Journal of Materials Chemistry A* 10 (2022): 23008–23014, https://doi.org/10.1039/D2TA06859A.

45. S. Zhao and F. Huang, "Weakly Solvating Few-Layer-Carbon Interface Toward High Initial Coulombic Efficiency and Cyclability Hard Carbon Anodes," *ACS Nano* 18 (2024): 1733.

46. Y. F. Tian, S. J. Tan, C. Yang, et al., "Tailoring Chemical Composition of Solid Electrolyte Interphase by Selective Dissolution for Long-Life Micron-Sized Silicon Anode," *Nature Communications* 14 (2023): 7247, https://doi.org/10.1038/s41467-023-43093-6.

47. C. Fang, J. Lau, D. Hubble, et al., "Large-Molecule Decomposition Products of Electrolytes and Additives Revealed by On-Electrode Chromatography and MALDI," *Joule* 5 (2021): 415–428, https://doi.org/10.1016/j.joule.2020.12.012.

48. E. Laviron, "General Expression of the Linear Potential Sweep Voltammogram in the Case of Diffusionless Electrochemical Systems," *Journal of Electroanalytical Chemistry and Interfacial Electrochemistry* 101 (1979): 19–28, https://doi.org/10.1016/S0022-0728(79)80075-3.

49. J. Zhang, X. Zhou, Q. Hu, et al., "Concentration-Induced Spontaneous Polymerization of Protic Ionic Liquids for Efficient In Situ Adhesion," *Nature Communications* 15 (2024): 4265, https://doi.org/10.1038/s41467-024-48561-1.

50. J. Zhao, W. Zhang, J. Hu, et al., "Research on the Risk of Thermal Runaway in the Industrial Process of Styrene Solution Polymerization," *Organic Process Research & Development* 25 (2021): 1366–1374, https://doi.org/10.1021/acs.oprd.0c00554.

51. C. Zhu, S. Chen, K. Li, et al., "Quantitative Analysis of the Structural Evolution in Si Anode via Multi-Scale Image Reconstruction," *Science Bulletin* 68 (2023): 408–416, https://doi.org/10.1016/j.scib.2023.01.032.

52. L. Wang, J. Yu, S. Li, et al., "Recent Advances in Interface Engineering of Silicon Anodes for Enhanced Lithium-Ion Battery Performance," *Energy Storage Materials* 66 (2024): 103243, https://doi.org/10.1016/j.ensm.2024.103243.

53. R. Zhang, Z. Xiao, Z. Lin, et al., "Unraveling the Fundamental Mechanism of Interface Conductive Network Influence on the Fast-Charging Performance of SiO-Based Anode for Lithium-Ion Batteries," *Nano-Micro Letters* 16 (2023): 43, https://doi.org/10.1007/s40820-023-01267-3.

Supporting Information

Additional supporting information can be found online in the Supporting Information section.

Supporting File: adma74536-sup-0001-SuppMat.pdf.

15214095, 0, Downloaded from https://advanced.onlinelibrary.wiley.com/doi/10.1002/adma.74536 by University Town Of Shenzhen, Wiley Online Library on [08/09/2026]. See the Terms and Conditions (https://onlinelibrary.wiley.com/terms-and-conditions) on Wiley Online Library for rules of use; OA articles are governed by the applicable Creative Commons License